Vectorial nonlinear propagation in silicon nanowire waveguides: polarization effects

Brian A. Daniel* and Govind P. Agrawal

Institute of Optics, University of Rochester, Rochester, New York 14627, USA
**Corresponding author: daniel@optics.rochester.edu*

Received January 28, 2010; accepted March 2, 2010;
posted March 8, 2010 (Doc. ID 123498); published April 20, 2010

A comprehensive theory is developed for describing the nonlinear propagation of optical pulses through silicon waveguides with nanoscale dimensions. Our theory includes not only the vectorial nature of optical modes but also the coupling between the transverse electric and magnetic modes occurring for arbitrarily polarized optical fields. We have studied the dependence of relevant nonlinear parameters on waveguide dimensions and found a class of waveguide geometries for which self-phase modulation can have a dramatic impact on the polarization state of the optical field. Self-induced polarization changes are studied for both the continuous and pulsed optical fields propagating in silicon waveguides. We also discuss the possibility of using these effects for intensity discrimination and pulse compression.

OCIS codes: 130.4310, 190.4390, 190.5940, 230.4320.

1. INTRODUCTION

Silicon-on-insulator (SOI) waveguides are attracting considerable attention because monolithic integration of such devices is likely to produce photonic integrated circuits relevant for future computing and communications technologies. The existing infrastructure for the SOI technology will allow such circuits to be fabricated at low cost. Nonlinear optical effects in SOI waveguides have also been studied in recent years [1–3] because an intrinsically large material nonlinearity of silicon, combined with the confinement of optical fields to nanoscale areas, allows them to be observed at modest power levels. All-optical switches, Raman lasers and amplifiers, parametric amplifiers, and a host of other devices have all been demonstrated in silicon waveguides [4–13].

Despite the considerable recent theoretical and experimental progress in the field of nonlinear silicon photonics, one area that has remained largely unexplored is the role that the state of polarization (SOP) of an optical field plays in nonlinear interactions. Part of the reason is related to use of the scalar approximation made commonly by assuming that the incident optical pulses excite either a transverse electric (TE) or a transverse magnetic (TM) mode of the waveguide but not both. In this paper we develop a theoretical framework for describing nonlinear phenomena in silicon nanowire waveguides which takes into account the full vectorial nature of the electromagnetic field. In Section 2 we present a rigorous derivation of the coupled-mode equations which describe the nonlinear interaction between the TE and TM modes. We quantify these effects in Section 3 through numerical calculations of the relevant nonlinear parameters and study their dependence on waveguide dimensions. In Section 4 we apply our vectorial theory to study the influence of self-phase modulation (SPM) on a continuous-wave (CW) field and show that the polarization state at the waveguide output becomes dependent on the optical power at the waveguide input. We then consider the propagation of pulsed optical fields and show that in this case the SPM results in a temporally varying polarization state at the waveguide output. The main results are summarized in Section 5.

2. THEORETICAL FRAMEWORK

As is well known [1], several linear and nonlinear processes affect the evolution of an optical pulse inside silicon nanowires. Two different yet related processes act to modify the phase of an optical field in silicon. The Kerr effect modifies the refractive index (and therefore the optical phase) in a quasi-instantaneous way. Coinciding with the Kerr effect is the process of two-photon absorption (TPA) which not only produces loss but also generates electron-hole pairs which build up the density of free carriers. These free carriers produce additional loss because they absorb light but they also modify the optical phase through changes in the refractive index. The generation and recombination of free carriers is characterized by a relatively slow response time (~1 ns). The Kerr and free-carrier processes lead to qualitatively different SPM effects that have been the subject of a number of theoretical and experimental studies [14–21]. However, these studies have considered the case in which the input pulse coupled into the waveguide is polarized linearly so that only a single spatial mode is excited.

A. Coupled Amplitude Equations

In this work we assume that an arbitrarily polarized optical field is launched such that it excites both the fundamental TE and TM modes of a silicon waveguide. The electric field $\mathbf{E}(\mathbf{r},t)$ at a point $\mathbf{r}$ inside the waveguide satisfies Maxwell's equations. Introducing the Fourier transform of a function $f(t)$ as

$$\tilde{f}(\omega) = \int_{-\infty}^{\infty} f(t) e^{i\omega t} dt, \tag{1}$$

the electric and magnetic fields in the frequency domain satisfy

$$\nabla \times \tilde{\mathbf{E}} = i\omega\mu_0 \tilde{\mathbf{H}}, \tag{2}$$

$$\nabla \times \tilde{\mathbf{H}} = -i\omega\varepsilon_0 n^2(x,y)\tilde{\mathbf{E}} - i\omega\tilde{\mathbf{P}}^{\mathrm{NL}}, \tag{3}$$

where $n(x,y)$ is the refractive index profile of the waveguide assumed to be uniform in the z direction. The material's nonlinear polarization $\tilde{\mathbf{P}}^{\mathrm{NL}}$ should not be confused with the SOP which is a property of the electric field and not the medium.

A common technique for solving Maxwell's equations makes use of optical modes supported by the waveguide in the absence of the nonlinear material polarization. The guided modes of Eqs. (2) and (3) can be found numerically for any waveguide geometry and are of the form

$$\tilde{\mathbf{E}}^{(k)}(\mathbf{r},\omega) = \mathbf{e}^{(k)}(x,y,\omega)\exp[i\beta^{(k)}(\omega)z],$$

$$\tilde{\mathbf{H}}^{(k)}(\mathbf{r},\omega) = \mathbf{h}^{(k)}(x,y,\omega)\exp[i\beta^{(k)}(\omega)z], \tag{4}$$

where $\beta^{(k)}$ is the propagation constant of the kth mode and the superscript k takes integer values 1 to M if the waveguide supports M guided modes. In general, the vectorial mode profile $\mathbf{e}^{(k)}(x,y,\omega)$ has nonzero e_x, e_y, and e_z components. In waveguides with core dimensions larger than the optical wavelength and a relatively low index contrast (such as optical fibers), the e_z component of a mode is negligible compared to either the e_x or e_y component. In the case of waveguides with sub-wavelength core dimensions and a high index contrast, this is no longer true and the complete vectorial nature of the optical mode must be retained for an accurate description [22–25]. SOI technology has a very high index contrast and it is also common to fabricate waveguides with nanometer-scale dimensions (dubbed "photonic nanowires"). For these reasons, we retain fully the vectorial nature of the optical modes in the following analysis.

We now consider the impact of the nonlinear term $\tilde{\mathbf{P}}^{\mathrm{NL}}$ in Eq. (2). Taking the curl of Eq. (2) and using the identity $\nabla\times\nabla\times\tilde{\mathbf{E}} = \nabla(\nabla\cdot\tilde{\mathbf{E}}) - \nabla^2\tilde{\mathbf{E}}$, we obtain

$$-\nabla(\nabla\cdot\tilde{\mathbf{E}}) + \nabla^2\tilde{\mathbf{E}} + \omega^2\mu_0\varepsilon_0 n^2(x,y)\tilde{\mathbf{E}} + \omega^2\mu_0\tilde{\mathbf{P}}^{\mathrm{NL}} = 0. \tag{5}$$

Although it is often assumed that $\nabla(\nabla\cdot\tilde{\mathbf{E}})\approx 0$, this approximation cannot be made for silicon nanowires as it amounts to neglecting the longitudinal field component E_z, which can be significant in such waveguides. We thus include this term in our theoretical description.

To solve Eq. (5), we assume that the input field excites only the fundamental quasi-TE and quasi-TM modes of the waveguide corresponding to $k=1$ and 2 in Eq. (4). In our notation, the quasi-TE mode ($k=1$) has a dominant e_x component, and the quasi-TM mode ($k=2$) has a dominant e_y component, where the y-axis is normal to the waveguide substrate. We now adopt the well-known coupled-mode approach in which the solution of Eq. (5) is expanded in terms of these two modes as

$$\tilde{\mathbf{E}}(\mathbf{r},\omega) \approx a_1(z,\omega)\mathbf{e}^{(1)}(x,y,\omega_0)e^{i\beta^{(1)}(\omega)z} + a_2(z,\omega)\mathbf{e}^{(2)}(x,y,\omega_0)e^{i\beta^{(2)}(\omega)z}, \tag{6}$$

where ω_0 is the carrier frequency and we approximate the transverse mode profiles ($\mathbf{e}^{(1)}$ and $\mathbf{e}^{(2)}$) to be independent of frequency over the bandwidth of the optical field. The z dependence of the mode amplitudes, a_1 and a_2, results from the mode coupling induced by the nonlinear polarization $\tilde{\mathbf{P}}^{\mathrm{NL}}$.

Using the preceding expansion in Eq. (5) and making the slowly varying envelope approximation, the mode amplitudes are found to satisfy (see the Appendix for its derivation)

$$\frac{da_k}{dz} = \frac{i\omega}{2N_k}\int\int \mathbf{e}^{*(k)}(x,y)\cdot\tilde{\mathbf{P}}^{\mathrm{NL}}(x,y,z)e^{-i\beta^{(k)}(\omega)z}dxdy, \tag{7}$$

where the integrals extend over the entire x-y plane and N_k, representing the power flow in the z direction, is defined as

$$N_k = \mathrm{Re}\left[\int\int (\mathbf{e}^{(k)}\times\mathbf{h}^{*(k)})\cdot\hat{\mathbf{z}}dxdy\right]. \tag{8}$$

This result is equivalent to the one in [26], where it is derived from the Lorentz reciprocity theorem.

We need to convert Eq. (7) to the time domain. For this purpose, it is useful to introduce a slowly varying mode amplitude as

$$\tilde{A}_k(z,\omega-\omega_0) = \sqrt{\frac{N_k}{2}}a_k(z,\omega)\exp\{i[\beta^{(k)}(\omega)-\beta_0^{(k)}]z\}, \tag{9}$$

where $\beta_0^{(k)}=\beta^{(k)}(\omega_0)$. Using Eq. (9) in Eq. (7), expanding $\beta^{(k)}(\omega)$ in a Taylor series around ω_0, and converting to the time domain by replacing $\omega-\omega_0$ with $i\partial/\partial t$, we find the following time-domain amplitude equation:

$$\frac{\partial A_k}{\partial z} = \left[\sum_{n=1}^{\infty} i^{n+1}\frac{\beta_n^{(k)}}{n!}\frac{\partial^n}{\partial t^n}\right]A_k + \exp[-i(\beta_0^{(k)}z-\omega_0 t)] \times\frac{i\omega_0}{2\sqrt{2N_k}}\int\int \mathbf{e}^{*(k)}(x,y)\cdot\mathbf{P}^{\mathrm{NL}}(x,y,z,t)dxdy, \tag{10}$$

where $\beta_n^{(k)}=\partial^n\beta^{(k)}/\partial\omega^n$ is the nth-order dispersion parameter of the waveguide at the frequency ω_0. Similarly using Eq. (9) in Eq. (6) and converting to the time domain results in the following expression for the electric field:

$$\mathbf{E}(\mathbf{r},t) \approx \sqrt{\frac{2}{N_1}}A_1(z,t)\mathbf{e}^{(1)}(x,y)\exp[i(\beta_0^{(1)}z-\omega_0 t)] + \sqrt{\frac{2}{N_2}}A_2(z,t)\mathbf{e}^{(2)}(x,y)\exp[i(\beta_0^{(2)}z-\omega_0 t)]. \tag{11}$$

It can be shown that $|A_k|^2$ is the optical power in the kth mode. The evaluation of the integrals in Eq. (10) requires

knowledge of the nonlinear polarization.

B. Third-Order Nonlinear Polarization

The nonlinear polarization $\mathbf{P}^{\mathrm{NL}}(\mathbf{r},t)$ in Eq. (10) has two independent contributions resulting from the third-order susceptibility and from free carriers generated by TPA, i.e.,

$$\mathbf{P}^{\mathrm{NL}}(\mathbf{r},t)=\mathbf{P}^{(3)}(\mathbf{r},t)+\mathbf{P}^{(fc)}(\mathbf{r},t). \tag{12}$$

Consider the contribution from the third-order polarization. If the bandwidth of the optical field is much less than the Raman shift in silicon (about 15.6 THz), the dominant contribution to the third-order susceptibility $\chi^{(3)}$ is due to electrons bound to silicon atoms in the crystal lattice. This electronic response is extremely fast and can be taken to be instantaneous. With this approximation, the μth component of the third-order polarization can be written as [27]

$$P_{\mu}^{(3)}(\mathbf{r},t)=\frac{3\varepsilon_0}{4}\sum_{\alpha,\beta,\gamma}\chi_{\mu\alpha\beta\gamma}^{(3)}(\omega_0;\omega_0,-\omega_0,\omega_0)\times E_{\alpha}(\mathbf{r},t)E_{\beta}^{*}(\mathbf{r},t)E_{\gamma}(\mathbf{r},t). \tag{13}$$

We use the Greek subscripts in this section for denoting the Cartesian components of a vector.

The third-order susceptibility of a silicon crystal depends on the orientation of the coordinate system relative to the crystallographic axes and can be written in the following general form [1]:

$$\chi_{\mu\alpha\beta\gamma}^{(3)}=\chi_c\left[\frac{\rho}{3}(\delta_{\mu\alpha}\delta_{\beta\gamma}+\delta_{\mu\beta}\delta_{\alpha\gamma}+\delta_{\mu\gamma}\delta_{\alpha\beta})+(1-\rho)\sum_{q}R_{q\mu}R_{q\alpha}R_{q\beta}R_{q\gamma}\right], \tag{14}$$

where $R_{\mu\nu}$ are the elements of a rotation matrix which maps the crystallographic coordinate system into one used to describe the waveguide modes and χ_c is the shorthand for the component $\chi_{1111}^{(3)}$ in the crystallographic coordinate system. It is common to fabricate SOI waveguides along the $[\bar{1}\bar{1}0]$ direction. In this case the rotation matrix in Eq. (14) is given by

$$\begin{pmatrix}R_{11}&R_{12}&R_{13}\\R_{21}&R_{22}&R_{23}\\R_{31}&R_{32}&R_{33}\end{pmatrix}=\frac{1}{\sqrt{2}}\begin{pmatrix}1&0&-1\\-1&0&-1\\0&\sqrt{2}&0\end{pmatrix}. \tag{15}$$

In this paper we only consider waveguides fabricated in the $[\bar{1}\bar{1}0]$ direction.

In Eq. (14), ρ is a parameter characterizing the anisotropic nature of the third-order susceptibility. At wavelengths near 1550 nm, $\rho\approx 1.27$ [1,28]. The quantity χ_c is related to the Kerr coefficient n_2 and the TPA coefficient β_{TPA} of an optical field polarized along a crystallographic axes as

$$\chi_c=\frac{4}{3}\varepsilon_0 c n_0^2 n_2(1+ir),\quad r=\frac{\beta_{\mathrm{TPA}}}{2k_0 n_2}, \tag{16}$$

where $k_0=\omega_0/c=2\pi/\lambda$, n_0 is the refractive index of bulk silicon, and r is a measure of the relative strength of the TPA process compared to the Kerr effect. Measurements of n_2 and β_{TPA} have been reported by a number of research groups [14–16,19,28,29], but they vary over a considerable range. In this paper, we use values from [29] where $n_2\approx 2.5\times 10^{-5}$ cm^2/GW and $\beta_{\mathrm{TPA}}=0.5$ cm/GW at wavelengths near 1550 nm. Using these values, $r\approx 0.25$.

We now consider the contribution of free carriers to the nonlinear polarization. As mentioned earlier, the TPA process generates electron-hole pairs, which in turn change the refractive index and the absorption coefficient within the silicon core of the waveguide. A commonly used semiempirical model assumes that the carrier-induced changes in the absorption coefficient and the refractive index at a wavelength of 1550 nm are of the form [1,30]

$$\Delta\alpha^{fc}=\sigma_a N, \tag{17}$$

$$\Delta n^{fc}=-\sigma_n^e N-(\sigma_n^h N)^{4/5}, \tag{18}$$

where N is the number density of electron-hole pairs, $\sigma_a=14.5\times 10^{-18}$ cm^2, $\sigma_n^e=8.8\times 10^{-22}$ cm^3, and $\sigma_n^h=4.6\times 10^{-22}$ cm^3. The material polarization, induced by the interaction of free carriers with the electric field, is then given by

$$\mathbf{P}^{(fc)}(\mathbf{r},t)=2\varepsilon_0 n_0[\Delta n^{fc}+(i/2k_0)\Delta\alpha^{fc}]\mathbf{E}(\mathbf{r},t). \tag{19}$$

C. Coupled-Mode Equations

We are now in a position to derive the coupled-mode equations. Using Eqs. (11), (10), and (13), the amplitude of the kth mode changes as

$$\frac{\partial A_k}{\partial z}=\left[\sum_{n=1}^{\infty}i^{n+1}\frac{\beta_n^{(k)}}{n!}\frac{\partial^n}{\partial t^n}\right]A_k+T_{3o}^k+T_{fc}^k, \tag{20}$$

where the three contributions are given by

$$T_{3o}^k=\sum_{lmn}\frac{3i\omega_0\varepsilon_0}{4(N_kN_lN_mN_n)^{1/2}}A_lA_m^*A_n\exp(i\Delta\beta_{klmn}z)\times\sum_{\mu\alpha\beta\gamma}\int\int\chi_{\mu\alpha\beta\gamma}^{(3)}e_{\mu}^{*(k)}e_{\alpha}^{(l)}e_{\beta}^{*(m)}e_{\gamma}^{(n)}dxdy, \tag{21}$$

$$T_{fc}^k=\sum_{l}i\frac{\omega_0\varepsilon_0 n_0}{(N_kN_l)^{1/2}}A_l\exp[i(\beta_0^{(l)}-\beta_0^{(k)})z]\times\int\int[\Delta n^{fc}+(i/2k_0)\Delta\alpha^{fc}]\mathbf{e}^{*(k)}\cdot\mathbf{e}^{(l)}dxdy, \tag{22}$$

where $\Delta\beta_{klmn}=-\beta_0^{(k)}+\beta_0^{(l)}-\beta_0^{(m)}+\beta_0^{(n)}$ represents a phase mismatch. The indices k,l,m,n take values 1 and 2 corresponding to the TE and TM modes, respectively.

Equation (20) describes the evolution of the mode amplitudes under very general conditions. Although it appears quite complicated, it can be simplified considerably in specific situations. For example, if one considers a highly birefringent waveguide, many of the terms can be

neglected because they oscillate rapidly in z (in the absence of phase matching). Alternatively, if we consider a silicon waveguide that exhibits reflection symmetry in the x and y directions (e.g., a rectangular silicon core surrounded on all sides by silica), then only four of the eight terms in the triple sum over l,m,n in Eq. (21) are nonvanishing and only the term for which $l=k$ is nonzero in Eq. (22). Because such silicon waveguides are commonly used and because their analysis is considerably simplified we focus on them in this paper. After considerable algebra, Eq. (20) leads to the following two coupled-mode equations for $k=1$ and 2:

$$\frac{\partial A_1}{\partial z} = \left[\sum_{n=1}^{\infty} i^{n+1}\frac{\beta_n^{(1)}}{n!}\frac{\partial^n}{\partial t^n}\right]A_1 + i\gamma_{11}(1+ir)|A_1|^2A_1 + i\gamma_{12}(1+ir) \times |A_2|^2A_1 + i\gamma'_{12}(1+ir)A_2^2A_1^* e^{-2ik_0\Delta nz} + ik_0\Gamma_1\frac{n_0}{\bar{n}_1} \times \left(\Delta n_1^{fc} + \frac{i}{2k_0}\Delta\alpha_1^{fc}\right)A_1 - \frac{\alpha_1}{2}A_1, \quad (23)$$

$$\frac{\partial A_2}{\partial z} = \left[\sum_{n=1}^{\infty} i^{n+1}\frac{\beta_n^{(2)}}{n!}\frac{\partial^n}{\partial t^n}\right]A_2 + i\gamma_{22}(1+ir)|A_2|^2A_2 + i\gamma_{12}(1+ir) \times |A_1|^2A_2 + i\gamma'_{12}(1+ir)A_1^2A_2^* e^{2ik_0\Delta nz} + ik_0\Gamma_2\frac{n_0}{\bar{n}_2} \times \left(\Delta n_2^{fc} + \frac{i}{2k_0}\Delta\alpha_2^{fc}\right)A_2 - \frac{\alpha_2}{2}A_2, \quad (24)$$

where $\bar{n}_j=\beta_0^{(j)}/k_0$ is the mode index and $\Delta n=\bar{n}_1-\bar{n}_2$ is the waveguide birefringence. The α_k terms have been added heuristically to account for internal waveguide losses.

The preceding coupled-mode equations introduce many new parameters that involve integration over the waveguide cross section. The most important are the four nonlinear parameters defined as

$$\gamma_{11} = \frac{n_0^2\Gamma_1^2}{\bar{n}_1^2\bar{a}_1}\eta_{11}k_0n_2, \quad \gamma_{22} = \frac{n_0^2\Gamma_2^2}{\bar{n}_2^2\bar{a}_2}\eta_{22}k_0n_2,$$

$$\gamma_{12} = \frac{2n_0^2\Gamma_1\Gamma_2\eta_{12}k_0n_2}{\bar{n}_1\bar{n}_2(\bar{a}_1\bar{a}_2)^{1/2}}, \quad \gamma'_{12} = \frac{n_0^2\Gamma_1\Gamma_2\eta'_{12}k_0n_2}{\bar{n}_1\bar{n}_2(\bar{a}_1\bar{a}_2)^{1/2}}, \quad (25)$$

where the effective mode area (EMA) of the mode with $k=1,2$ is defined as

$$\bar{a}_k = \left(\int\int |\mathbf{e}^{(k)}|^2dxdy\right)^2 \Big/ \left(\int\int (|\mathbf{e}^{(k)}|^2)^2dxdy\right). \quad (26)$$

The real dimensionless parameter Γ_k measures the relative contribution of the longitudinal component of the electric fields associated with the two modes and is defined as

$$\Gamma_k = \frac{\int\int |\mathbf{e}^{(k)}|^2dxdy}{\int\int |\mathbf{e}_T^{(k)}|^2 + (\beta^{(k)})^{-1}\mathrm{Im}(\mathbf{e}_T^{(k)}\cdot\nabla_T e_z^{k*})dxdy}. \quad (27)$$

Numerically, $\Gamma_k\geq 1$ and reduces to 1 only for a purely transverse mode field. We refer to it as the longitudinal enhancement factor (LEF) because it enhances the nonlinear effects in silicon nanowires [2].

The parameters η_{lm} are also real dimensionless parameters defined as

$$\eta_{lm} = \sum_{\mu\alpha\beta\gamma}\frac{\chi_c^{-1}\int\int\chi^{(3)}_{\mu\alpha\beta\gamma}e_\mu^{*(l)}e_\alpha^{(l)}e_\beta^{*(m)}e_\gamma^{(m)}dxdy}{\left[\int\int(|\mathbf{e}^{(l)}|^2)^2dxdy\int\int(|\mathbf{e}^{(m)}|^2)^2dxdy\right]^{1/2}}, \quad (28)$$

$$\eta'_{12} = \sum_{\mu\alpha\beta\gamma}\frac{\chi_c^{-1}\int\int\chi^{(3)}_{\mu\alpha\beta\gamma}e_\mu^{*(1)}e_\alpha^{(2)}e_\beta^{*(1)}e_\gamma^{(2)}dxdy}{\left[\int\int(|\mathbf{e}^{(l)}|^2)^2dxdy\int\int(|\mathbf{e}^{(m)}|^2)^2dxdy\right]^{1/2}}. \quad (29)$$

They are a measure of the way in which the TE and TM vectorial modes interact through the anisotropic third-order susceptibility. We refer to these terms as the nonlinear overlap factors (NOFs). Finally, the subscript k in Δn_k^{fc} and $\Delta\alpha_k^{fc}$ in the free-carrier terms in the coupled-mode equations indicate that these quantities are evaluated as overlap integrals with the transverse mode profiles, i.e.,

$$\Delta n_k^{fc} = \int\int \Delta n^{fc}(x,y)|\mathbf{e}^{(k)}|^2dxdy \Big/ \left(\int\int |\mathbf{e}^{(k)}|^2dxdy\right),$$

$$\Delta\alpha_k^{fc} = \int\int \Delta\alpha^{fc}(x,y)|\mathbf{e}^{(k)}|^2dxdy \Big/ \left(\int\int |\mathbf{e}^{(k)}|^2dxdy\right).$$

Coupled-mode equations (23) and (24) describe the evolution of the fundamental TE and TM modes inside a silicon nanowire. We use them in this paper to discuss interesting polarization effects. However, before doing that, we compare our formalism with two other studies that also consider the vectorial nature of optical modes. Chen *et al.* [31] presented a theory for nonlinear propagation in silicon nanowires and include the Kerr nonlinearity, TPA, Raman interaction, and free-carrier effects. Afshar and Monro [23] developed a similar vectorial theory but they do not include the free-carrier effects as their emphasis is on glass waveguides. The expressions we derive for the coupled-mode equations and the nonlinear parameters in Eq. (25) can be compared with their results in certain limits.

In Chen *et al.* a theory is developed to describe the propagation of linearly polarized pump and Stokes pulses interacting through Raman amplification. In the case that the Stokes field is absent their theory is comparable to ours when we consider only a single spatial mode being excited [i.e., $A_2=0$ in Eqs. (23) and (24)]. In this case our theories agree. A demonstration of this agreement requires the use of theorems concerning waveguide modes from [26].

In the case of an isotropic medium ($\rho=1$), our expressions for the γ parameters in Eq. (25) reduce to those in [23]. In this case, Eqs. (23) and (24) can be further simplified to describe the TE and TM modes of a single-mode optical fiber if we approximate the modes as being trans-

verse ($e_z^{(k)} \approx 0$). In this approximation, they reduce to the well-known expressions for optical fibers [32].

3. GEOMETRIC DEPENDENCE OF NONLINEAR PARAMETERS

As seen from Eqs. (25)–(28), the effective nonlinear parameters that govern the pulse propagation in silicon nanowires depend on waveguide dimensions through the EMAs $\bar{a}_k$, the LEFs Γ_k, and the NOFs η_{kl}, where $k=1$ and 2 for the TE and TM modes, respectively. In this section we study the geometric dependence of these quantities by focusing on waveguides whose rectangular silicon core is surrounded on all sides by silica, as shown schematically in Fig. 1. Since no exact analytic solution exists for the vectorial modes of Eq. (4) for such waveguides, we employ a numerical technique based on the full-vector finite-difference method described in [33] to calculate the propagation constants $\beta^{(k)}$ and the vectorial mode profiles $\mathbf{e}^{(k)}(x,y)$ of the fundamental TE and TM modes of the waveguide. In the following numerical calculations, we assume that the incident optical pulse has a carrier wavelength of 1550 nm.

The nonlinear parameter of a mode depends strongly on the dimension of the waveguide that is orthogonal to the mode's polarization direction. For example, the nonlinear parameter of the TE mode, γ_{11}, depends strongly on the height of a waveguide, but only weakly on its width. This is evident from Fig. 2 which shows γ_{11} as a function of waveguide dimensions. As a result of the inherent symmetry of our waveguide in Fig. 1, the dependence of the nonlinear parameter of the TM mode (γ_{22}) on the waveguide width is qualitatively similar to the dependence of γ_{11} on the waveguide height. In fact, if silicon were an isotropic medium (i.e., if $\rho=1$), this would also hold quantitatively. Since silicon is anisotropic ($\rho \approx 1.27$ near 1550 nm), there are quantitative differences between the TE and TM modes.

The underlying reason for why γ_{11} depends primarily on the waveguide height is the polarization dependence of modal confinement. Conceptually, the confinement of a mode to the waveguide core is very sensitive to the dimension of the waveguide along which it is polarized. As this dimension decreases the degree of modal confinement does as well. As a result, the effective area $\overline{a_k}$ of the mode defined in Eq. (26) depends only weakly on the dimension along which it is polarized. However, the EMA is strongly dependent on the dimension orthogonal to the mode's polarization direction and any change in this dimension results in a proportional change in the effective area. This is evident from Fig. 3 where we plot the EMAs of the fundamental TE and TM modes against the waveguide height for a fixed width of 500 nm. As the waveguide height reaches the effective optical wavelength in silicon ($\lambda/n \approx 440$ nm) the EMA of the TM mode reaches a minimum. A further decrease in the waveguide height results in an increase in $\bar{a}_2$ rather than a decrease. The EMA of the TE mode, however, decreases monotonically with the waveguide height down to dimensions at which the TM mode no longer exists [when the height $h \approx \lambda/(2n)$]. Clearly, nanowire waveguides will exhibit strong polarization dependence in their nonlinear behavior because of this feature.

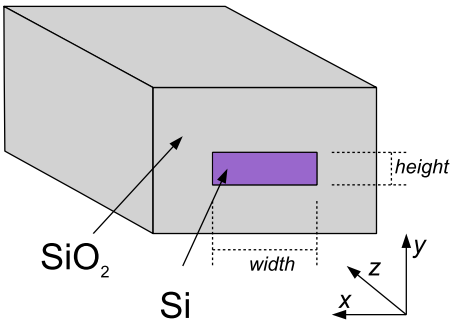

Fig. 1. (Color online) Schematic of the waveguide geometry employed.

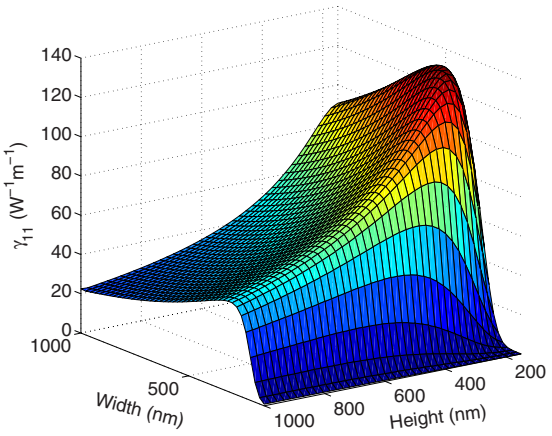

Fig. 2. (Color online) γ_{11} as a function of waveguide width and height at the 1550 nm wavelength.

The EMA is not the only quantity in Eq. (25) related to modal confinement. The NOFs (η_{11}, η_{22}, and η_{12}) measure how effectively the vectorial modes overlap with the third-order susceptibility, which is confined to the silicon core (we ignore the silica nonlinearity in the cladding as it is >100 times smaller). A waveguide mode with a longer tail into the cladding region will have a smaller η parameter. Indeed, we see in Fig. 4 that η_{22} and η_{12} depend strongly on the waveguide height. As the TM mode begins

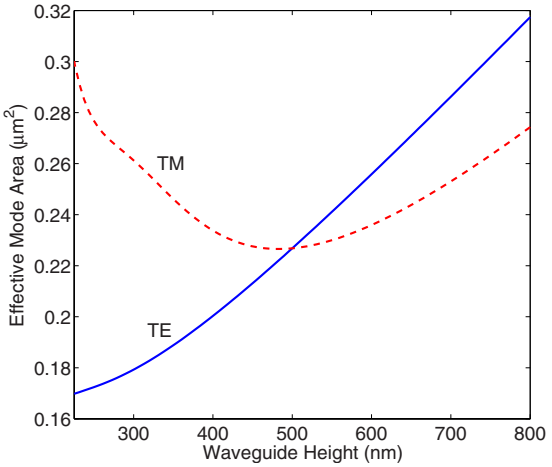

Fig. 3. (Color online) EMAs, $\bar{a}_1$ and $\bar{a}_2$, as a function of waveguide height for a fixed waveguide width of 500 nm at $\lambda=1550$ nm.

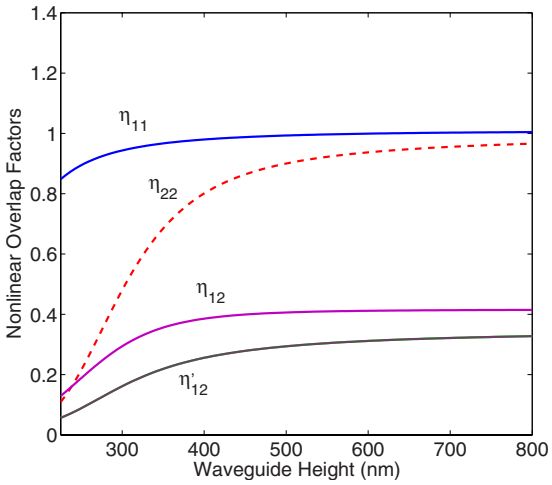

Fig. 4. (Color online) η_{11}, η_{22}, and η_{12} as a function of waveguide height for a fixed waveguide width of 500 nm at $\lambda = 1550$ nm.

to lose its confinement for $h < \lambda/n$, both of these quantities become smaller. The nonlinear parameter γ_{22} is therefore reduced not only by an increase in its effective area but also by a reduction in η_{22}. The NOF for the TE mode (η_{11}), however, is relatively independent of the waveguide height. Notice that even for relatively large waveguides η_{11} exceeds η_{22} by about 15% as a result of the anisotropy of silicon's third-order susceptibility. If silicon were an isotropic medium, we would find $\eta_{22} = \eta_{11}$ and $\eta_{12} = \eta_{11}/3$ in this situation, similar to the case of optical fibers.

While the modal confinement can be understood as the underlying reason why the nonlinear parameters depend on waveguide dimensions as they do, we also need to consider the geometric dependence of the LEFs Γ_k and the effective mode indices $\bar{n}_k$. These quantities are plotted in Fig. 5 as a function of the waveguide height and they act to enhance the effective nonlinear parameters for nanowire waveguides with dimensions $< \lambda/n$. As the waveguide height decreases below λ/n, the LEF Γ_2 for the TM mode becomes larger by as much as 60%. This enhancement is related to the increasing magnitude of the longitudinal field component e_z for narrower waveguides. Figure 5 also shows that the effective index of the TM mode ($\bar{n}_2$) become notably smaller for nanowire waveguides with subwavelength heights. For such geometries the evanescence of the TM mode into the silica cladding where the material index is much lower results in smaller effective indices. Since the nonlinear parameter γ_{22} is inversely proportional to $\bar{n}_2^2$, and directly proportional to Γ_2, both of these parameters act to enhance it.

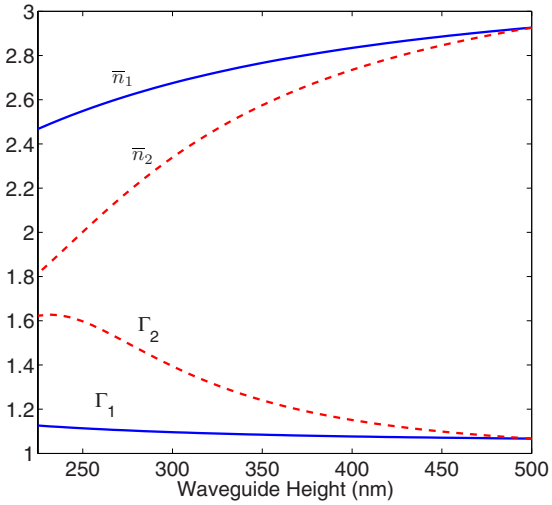

Fig. 5. (Color online) LEFs and effective mode indices as a function of waveguide height for a fixed waveguide width of 500 nm at $\lambda = 1550$ nm.

Since the TM mode's EMA and NOF reduce γ_{22} while its LEF and $\bar{n}_2$ increase it for narrow waveguides, their cumulative behavior determines the overall impact of the waveguide geometry. Figure 6 shows the dependence of the γ parameters on the waveguide height. As seen there, γ_{11} (corresponding to the TE mode) increases with a reduction in the waveguide height. In contrast, γ_{22} increases initially because of an enhanced LEF and a lower effective mode index but is ultimately reduced for waveguides with subwavelength heights as a result of weak modal confinement. The same behavior would occur as the waveguide width is reduced for γ_{11}.

The influence of free carriers on the optical field is also affected by waveguide geometry. As was seen in Section 2, when the refractive index of the silicon material changes by Δn^{fc}, the resulting change in the effective index of a waveguide mode is modified by a number of geometrical parameters. It follows from the last term in Eqs. (23) and (24) that the effective free-carrier change in the mode index is given by

$$\Delta \bar{n}_k^{fc} = \frac{n_0}{\bar{n}_k} \Gamma_k \Delta n_k^{fc} \approx \frac{n_0}{\bar{n}_k} \Gamma_k \Pi_k \Delta n^{fc} = B_k \Delta n_k^{fc}, \tag{30}$$

where we approximated Δn^{fc} as being independent of x and y within the core region of the waveguide and introduced Π_k as the confinement factor for the kth mode as

$$\Pi_k = \int\int_{\mathrm{Si}} |\mathbf{e}^{(k)}|^2 dxdy \Big/ \left(\int\int |\mathbf{e}^{(k)}|^2 dxdy \right). \tag{31}$$

The quantity B_k is the index overlap factor for the kth mode. Figure 7 shows the dependence of B_1 and B_2 on the

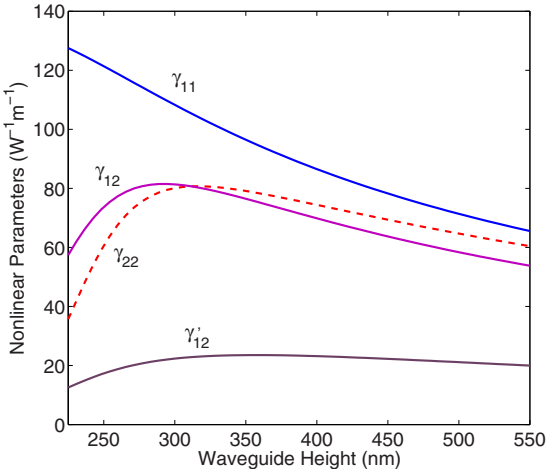

Fig. 6. (Color online) Nonlinear parameters as a function of waveguide height for a fixed waveguide width of 500 nm at $\lambda = 1550$ nm.

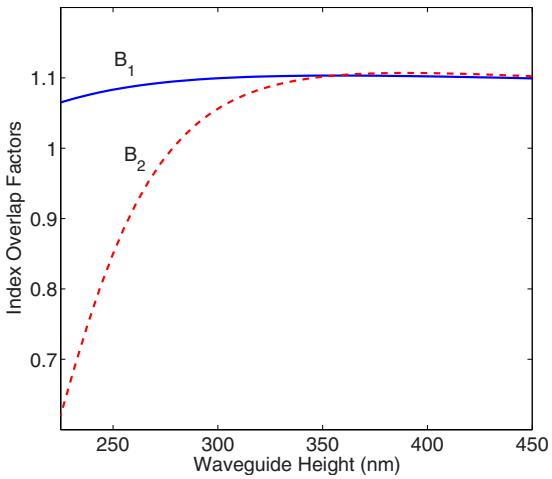

Fig. 7. (Color online) Factors B_1 and B_2 as a function of waveguide height for a fixed waveguide width of 500 nm at $\lambda = 1550$ nm.

waveguide height. For heights <300 nm B_2 becomes smaller because of the weaker modal confinement of the TM mode.

There are waveguide geometries for which free carriers change not only the refractive index but also the birefringence of the waveguide. Equation (30) indicates that this birefringence change is given by $(B_1 - B_2)\Delta n^{fc}$. Figure 7 shows that the modal birefringence introduced by free carriers can be as much as 30% of the free-carrier-induced change in the material's refractive index. The implication is that for certain waveguide geometries the presence of free carriers will have a significant impact on the polarization state of the optical field. This issue is explored further in the next section.

4. SELF-PHASE MODULATION AND STATE OF POLARIZATION

When an intense optical pulse or a CW beam propagates through a silicon waveguide, its phase is modified by the Kerr effect as well as by index changes resulting from TPA-generated free carriers [1]. In the case of an asymmetric waveguide whose width or height is smaller than the optical wavelength (λ/n), both the Kerr and free-carrier effects can lead to a significant change in waveguide birefringence. The SOP of the optical field at the output of the waveguide can then be quite different from the SOP of the input field itself. In this section we consider these SPM-induced changes in the SOP of an optical field.

The SOP of a plane wave is determined by the relative phase between the two transverse field components E_x and E_y and their relative magnitudes [34]. The SOP inside the waveguide is more complicated than the SOP of a plane wave for two reasons. First, as we have already shown, there can be a significant longitudinal field component E_z inside a silicon nanowire. Second, the mode profiles of the TE and TM modes have different dependence on the transverse dimensions x and y so that the relative magnitude of the field components E_x and E_y varies with these dimensions. In order to simplify the situation we describe the SOP in the waveguide in a manner analogous to a plane wave. We use the relation $A_k = \sqrt{P_k}e^{i\phi_k}$, where P_k is the optical power in the kth mode and ϕ_k contributes to its phase. The SOP is determined by the power in each mode and the relative phase δ between the two modes. According to Eq. (11) this relative phase has two distinct contributions,

$$\delta = \delta_L + \delta_{NL}, \tag{32}$$

where the linear and nonlinear contributions for a waveguide of length L are given by

$$\delta_L = (\beta_0^{(1)} - \beta_0^{(2)})L, \tag{33}$$

$$\delta_{NL} = \phi_1(L) - \phi_2(L). \tag{34}$$

The linear contribution δ_L results solely from waveguide birefringence. The nonlinear contribution δ_{NL} results from nonlinear effects inside the waveguide as well as from walk off, dispersion, and the SOP of the field at the waveguide input. For low-power optical waves, δ will not be influenced by the Kerr effect or by TPA-generated free carriers, and the output SOP is different from the input SOP only because of the linear effects occurring in the waveguide. As the optical power increases δ_{NL} begins to change as a result of the nonlinear effects resulting in power-dependent changes in the output SOP of the optical field.

We characterize the SOP through Stokes parameters defined as [32,34]

$$S_0 = |A_1|^2 + |A_2|^2, \quad S_1 = |A_1|^2 - |A_2|^2,$$

$$S_2 = \mathrm{Re}(2A_1A_2^* e^{i\delta_L}), \quad S_3 = \mathrm{Im}(2A_1A_2^* e^{i\delta_L}). \tag{35}$$

Notice that the nonlinear contribution to the differential phase shift is included automatically through the complex field amplitudes. The linear contribution is extremely sensitive to the waveguide length L and differs from waveguide to waveguide. To isolate the nonlinear effects, we assume that $\delta_L = 2m\pi$ for some integer m in the following analysis.

We calculate the Stokes parameters by solving coupled-mode equations (23) and (24) numerically for a nanowire waveguide with 500 nm width, 240 nm height, and 2 cm length. All of the relevant nonlinear parameters can be obtained from the figures presented in Section 3. We assume linear losses of 3 dB/cm for both the TE and TM modes. Because the waveguide under consideration is highly birefringent, the terms containing $\exp(\pm 2ik_0\Delta nz)$ in Eqs. (23) and (24) can be neglected as they oscillate rapidly in z. However, their solution requires a rate equation describing the dynamics of carrier density N. This equation is of the form [1]

$$\frac{dN}{dt} = G - \frac{N}{\tau_{fc}}, \tag{36}$$

where τ_{fc} is the free-carrier lifetime taken to be 1 ns in this study. If the electron-hole pairs are created by TPA alone, their generation rate is given by [1]

$$G = \frac{r}{A_c \hbar \omega_0}(\gamma_{11}|A_1|^4 + \gamma_{22}|A_2|^4 + 2\gamma_{12}|A_1 A_2|^2), \quad (37)$$

where A_c is the cross-section area of the silicon core.

A. Case of a CW Input Beam

In the case of a CW beam, carrier density N is given by the steady-state solution of Eq. (36). Moreover, all the time derivatives in Eqs. (23) and (24) vanish since the envelopes A_1 and A_2 do not vary with time. After dropping these terms, we can write these equations in terms of the mode powers and the nonlinear differential phase shift as follows:

$$\frac{dP_1}{dz} = -2\gamma_{11} r P_1^2 - 2\gamma_{12} r P_1 P_2 - B_1 \Delta\alpha^{fc} P_1 - \alpha_1 P_1, \quad (38)$$

$$\frac{dP_2}{dz} = -2\gamma_{22} r P_2^2 - 2\gamma_{12} r P_1 P_2 - B_2 \Delta\alpha^{fc} P_2 - \alpha_2 P_2, \quad (39)$$

$$\frac{d\delta_{\mathrm{NL}}}{dz} = (\gamma_{11} - \gamma_{12})P_1 + (\gamma_{12} - \gamma_{22})P_2 + k_0(B_1 - B_2)\Delta n^{fc}. \quad (40)$$

It is clear from phase equation (40) that both the SPM and free carriers affect the differential phase shift. In general, the Kerr effect acts to increase the waveguide birefringence, whereas free carriers reduce it because of the negative value of Δn^{fc}. In the case of CW light, free-carrier effects dominate because of the buildup of a steady population of free carriers [1].

Figure 8 shows how the Stokes parameters at the output of the waveguide depend on the power for an input field polarized at 45° from the x axis so that both the TE and TM modes are equally excited. The output field remains linearly polarized at +45° at lower powers ($S_2/S_0 = 1$) but becomes left-circularly polarized at an input power of 200 mW after passing through elliptical SOPs. With a further increase in power, it becomes again elliptically polarized and acquires a −45° linear SOP when the input power reaches 400 mW. A right-circularly polarized state occurs at a power level of 700 mW. These polarization changes result mostly from the presence of free carriers.

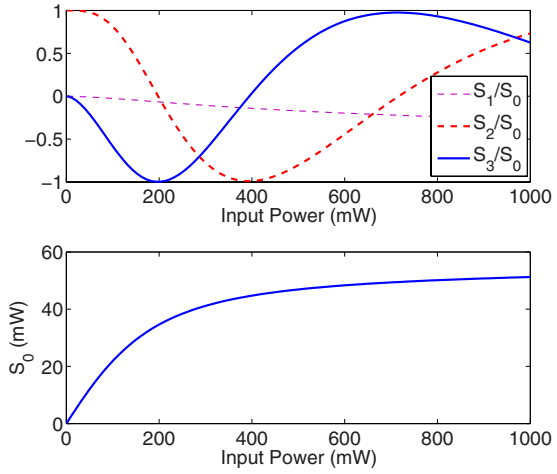

Fig. 8. (Color online) Stokes parameters as a function of the input power of a CW beam propagating through a 2-cm-long waveguide at λ = 1550 nm.

From a practical standpoint, the nonlinear rotation of the field's SOP can be used to make an intensity discriminator if a linear polarizer acting as an analyzer is placed at the waveguide output. Such a device would work for both CW beams and quasi-CW pulses whose temporal widths are much longer than the free-carrier lifetime. This lifetime is typically ~1 ns but it can be reduced by electrically biasing a waveguide built in a p-i-n structure. As an example, consider nanosecond pulses that have noise imposed on them by an amplifier (or some other means). When such a pulse is sent through a silicon nanowire, the noise will not experience any change in its SOP because of its relatively low power, but the SOP of the central part of the pulse can be rotated by 90°. An analyzer at the output end will let the pulse pass but will block the noise.

B. Case of Picosecond Input Pulses

The case of an optical pulse differs from the CW case in that the density of electron-hole pairs N (and therefore the resulting index changes) change dynamically along the pulse. The SPM induced by the Kerr effect also changes with time and leads to considerable chirping of the pulse. As a result, one expects that the SOP of a pulse, although uniform initially along the entire pulse duration, will become nonuniform, and different parts of the pulse would exhibit different SOPs.

The main difference in the pulsed case is that we now have to keep the time derivatives in Eqs. (23) and (24) as well as in carrier-density equation (36). To simplify coupled-mode equations (23) and (24), we retain only the first- and second-order time derivatives and neglect all higher-order dispersion terms. We find the group indices of the TE and TM modes numerically to be 4.199 and 4.270, respectively. We also calculate β_2 for the TE and TM modes to be −0.857 and 16.431 ps^2/m, respectively.

We solve Eqs. (23) and (24) with the symmetric split-step Fourier method. We consider a waveguide with the same parameters as in the CW case. Figure 9 shows the Stokes parameters as a function of time at the output of the waveguide for a 15-ps input Gaussian pulse polarized linearly at 45° and launched with 6.75 W peak power. The carrier density N is initially zero but it builds up after the front end of the pulse enters the waveguide and takes its maximum value after the trailing edge has passed away. Such temporal changes in N cause a time-dependent birefringence through the index changes induced by free carriers which, in turn, causes temporal oscillations in the Stokes parameters seen in Fig. 9. In particular, there is a temporal region of the pulse where the polarization state switches completely from a +45° linear SOP to a −45° one.

One implication of the observed polarization dynamics is the possibility for pulse compression. Also shown in Fig. 9 is the optical power of the output pulse after it has been passed through a linear analyzer oriented orthogonal to the input SOP of the pulse (dashed curve). The original 15-ps pulse is compressed down to a width of around 4 ps leading to a compression factor of about 3.75. At higher

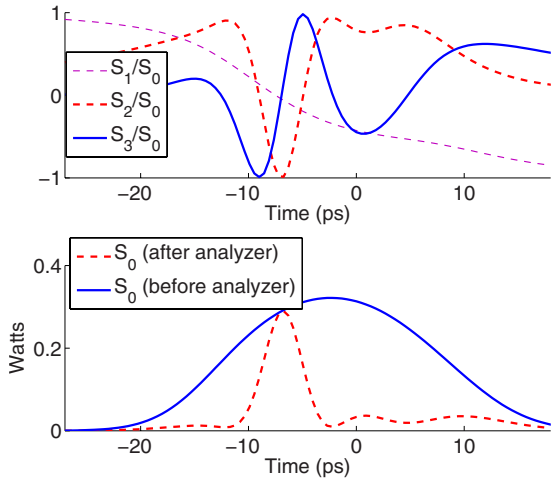

Fig. 9. (Color online) Stokes parameters versus time at the output of a 2-cm-long waveguide for a 15-ps input Gaussian pulse, polarized linearly at 45° and launched with 6.75 W peak power. The bottom plot shows optical power after the output pulse passes through a −45° linear analyzer. The center wavelength of the input pulse is 1550 nm.

powers, the SOP at the waveguide output will oscillate more rapidly due to enhanced free-carrier index changes and results at the output of the analyzer in a splitting of a single pulse into multiple distinct pulses of shorter temporal width.

5. CONCLUSIONS

We have developed a comprehensive theory for describing the nonlinear propagation of optical pulses through silicon waveguides with nanoscale dimensions. Our theory includes not only the vectorial nature of optical modes but also the coupling between the TE and TM modes that occurs for arbitrarily polarized optical fields. We have studied the dependence of relevant nonlinear parameters on waveguide dimensions and found a class of waveguide geometries for which self-phase modulation can have a dramatic impact on the polarization state of the optical field. Self-induced changes in the polarization state have been studied for both CW and pulsed fields propagating in silicon nanowire waveguides. We also discussed the possibility of using these effects for intensity discrimination and pulse compression. Our theoretical formalism should be useful for novel device applications making use of nonlinear polarization effects in silicon nanowire waveguides.

APPENDIX A: DERIVATION OF THE MODE-AMPLITUDE PERTURBATION EQUATION

To derive Eq. (7) from Eq. (5), it is useful to separate the transverse and longitudinal parts of the optical field by writing the electric and magnetic fields in the form

$$\mathbf{E}^{(k)} = \mathbf{E}_T^{(k)} + E_z^{(k)}\hat{\mathbf{z}}, \quad \mathbf{H}^{(k)} = \mathbf{H}_T^{(k)} + H_z^{(k)}\hat{\mathbf{z}}, \tag{A1}$$

where $\mathbf{E}_T^{(k)} = E_x^{(k)}\hat{\mathbf{x}} + E_y^{(k)}\hat{\mathbf{y}}$. Inserting Eq. (6) into Eq. (5), making the slowly varying envelope approximation by neglecting the second derivative of a_k, and using the fact that $\mathbf{E}^{(k)}$ is a solution of Eq. (5) when $\tilde{\mathbf{P}}^{\mathrm{NL}} = 0$, we obtain

$$\sum_{k=1}^{M} \frac{da_k}{dz}[2i\beta^{(k)}\mathbf{E}_T^{(k)} - \nabla_T E_z^{(k)} - (\nabla_T \cdot \mathbf{E}_T^{(k)})\hat{\mathbf{z}}] = -\omega^2\mu_0\tilde{\mathbf{P}}^{\mathrm{NL}}, \tag{A2}$$

where M is the total number of modes in the general case of a multimode waveguide.

If we multiply Eq. (A2) with $\mathbf{E}^{*(m)}$ and integrate over the transverse dimensions, we obtain

$$\sum_l \frac{da_l}{dz}\int\int [2i\beta^{(m)}\mathbf{E}_T^{*(m)}\cdot\mathbf{E}_T^{(l)} - \mathbf{E}_T^{*(m)}\cdot\nabla_T E_{lz} - \nabla_T\cdot(E_T^{*(m)}\mathbf{E}_T^{(l)}) + \mathbf{E}_T^{*(l)}\cdot\nabla_T E_z^{*(m)}]dxdy = -\omega^2\mu_0\int\int \mathbf{E}^{*(m)}\cdot\tilde{\mathbf{P}}^{\mathrm{NL}}dxdy, \tag{A3}$$

where we used the product rule

$$(\nabla_T\cdot\mathbf{E}_T^{(l)})E_z^{*(m)} = \nabla_T\cdot(E_z^{*(m)}\mathbf{E}_T^{(l)}) - \mathbf{E}_T^{(l)}\cdot\nabla_T E_z^{*(m)}.$$

Modes with propagation constants $\beta^{(k)} \neq \beta^{(m)}$ have been dropped from the sum as they are not phase-matched with the mth mode and introduce terms oscillating rapidly with z.

Consider the term $\int\int\nabla_T\cdot(E_z^{*(m)}\mathbf{E}_T^{(l)})dxdy$. From Gauss's theorem, the integral over a finite transverse region R is equal to a line integral around the boundary of R:

$$\int\int_R \nabla_T\cdot(E_z^{*(m)}\mathbf{E}_T^{(l)})dxdy = \oint_R E_z^{*(m)}\mathbf{E}_T^{(l)}\cdot d\ell_\perp. \tag{A4}$$

As the region of integration is taken to extend the entire transverse plane, the right side of this equation vanishes because all guided modes decay exponentially in the cladding. Thus, Eq. (A3) simplifies to

$$\sum_l \frac{da_l}{dz}\int\int [2i\beta^{(m)}\mathbf{E}_T^{*(m)}\cdot\mathbf{E}_T^{(l)} - \mathbf{E}_T^{*(m)}\cdot\nabla_T E_z^{(l)} + \mathbf{E}_T^{(l)}\cdot\nabla_T E_z^{(m)*}]dxdy = -\omega^2\mu_0\int\int \mathbf{E}^{*(m)}\cdot\tilde{\mathbf{P}}^{\mathrm{NL}}dxdy. \tag{A5}$$

We now use the following expression from [23]:

$$2i\beta^{(m)}\mathbf{E}_T^{*(m)}\cdot\mathbf{E}_T^{(l)} - \mathbf{E}_T^{*(m)}\cdot\nabla_T E_z^{(l)} + \mathbf{E}_T^{(l)}\cdot\nabla_T E_z^{*(m)} = i\omega\mu_0[\mathbf{E}^{(l)}\times\mathbf{H}^{*(m)} + \mathbf{E}^{*(m)}\times\mathbf{H}^{(l)}]\cdot\hat{\mathbf{z}}. \tag{A6}$$

With this identity and Eq. (4), Eq. (A5) becomes

$$\sum_l \frac{da_l}{dz}\int\int [\mathbf{e}^{(l)}\times\mathbf{h}^{*(m)} + \mathbf{e}^{*(m)}\times\mathbf{h}^{(l)}]\cdot\hat{\mathbf{z}}dxdy = i\omega\int\int \mathbf{e}^{*(m)}\cdot\tilde{\mathbf{P}}^{\mathrm{NL}}\exp[-i\beta^{(m)}z]dxdy. \tag{A7}$$

Assuming that all modes are orthogonal to each other, or they have been made orthogonal using the well-known Gram–Schmidt process, we can use the relation

$$\int\int [\mathbf{e}^{(l)} \times \mathbf{h}^{*(m)} + \mathbf{e}^{*(m)} \times \mathbf{h}^{(l)}] \cdot \hat{\mathbf{z}} dxdy = 2N_m \delta_{lm},$$

where N_m is defined in Eq. (8). Using it, we finally obtain

$$\frac{da_m}{dz} = \frac{i\omega}{2N_m} \int\int \mathbf{e}^{*(m)} \cdot \tilde{\mathbf{P}}^{\mathrm{NL}} \exp[-i\beta^{(m)} z] dxdy. \quad \text{(A8)}$$

ACKNOWLEDGMENTS

This work was supported in part by the National Science Foundation (NSF) award ECCS-0801772. We thank P. M. Fauchet and M. Premaratne for their support of this work.

REFERENCES

1. Q. Lin, O. J. Painter, and G. P. Agrawal, "Nonlinear optical phenomena in silicon waveguides: modeling and applications," Opt. Express **15**, 16604–16644 (2007).
2. R. M. Osgood, Jr., N. C. Panoiu, J. I. Dadap, X. Liu, X. Chen, I.-W. Hsieh, E. Dulkeith, W. M. Green, and Y. A. Vlasov, "Engineering nonlinearities in nanoscale optical systems: physics and applications in dispersion-engineered silicon nanophotonic wires," Adv. Opt. Photon. **1**, 162–235 (2009).
3. I. D. Rukhlenko, M. Premaratne, and G. P. Agrawal, "Nonlinear silicon photonics: analytical tools," IEEE J. Sel. Top. Quantum Electron. **16**, 200–215 (2010).
4. O. Boyraz and B. Jalali, "Demonstration of a silicon Raman laser," Opt. Express **12**, 5269–5273 (2004).
5. H. Rong, S. Xu, O. Cohen, O. Raday, M. Lee, V. Sih, and M. Paniccia, "A cascaded silicon Raman laser," Nat. Photonics **2**, 170–174 (2008).
6. O. Boyraz, P. Koonath, V. Raghunathan, and B. Jalali, "All optical switching and continuum generation in silicon waveguides," Opt. Express **12**, 4094–4102 (2004).
7. R. Dekker, A. Driessen, T. Wahlbrink, C. Moormann, J. Niehusmann, and M. Först, "Ultrafast Kerr-induced all-optical wavelength conversion in silicon waveguides using 1.55 μm femtosecond pulses," Opt. Express **14**, 8336–8346 (2006).
8. M. A. Foster, A. C. Turner, J. E. Sharping, B. S. Schmidt, M. Lipson, and A. L. Gaeta, "Broad-band optical parametric gain on a silicon photonic chip," Nature **441**, 960–963 (2006).
9. Y. Kuo, H. Rong, V. Sih, S. Xu, M. Paniccia, and O. Cohen, "Demonstration of wavelength conversion at 40 Gb/s data rate in silicon waveguides," Opt. Express **14**, 11721–11726 (2006).
10. S. Ayotte, H. Rong, S. Xu, O. Cohen, and M. J. Paniccia, "Multichannel dispersion compensation using a silicon waveguide-based optical phase conjugator," Opt. Lett. **32**, 2393–2395 (2007).
11. R. Salem, M. A. Foster, A. C. Turner, D. F. Geraghty, M. Lipson, and A. L. Gaeta, "Signal regeneration using low-power four-wave mixing on silicon chip," Nat. Photonics **2**, 35–38 (2008).
12. M. A. Foster, R. Salem, D. F. Geraghty, A. C. Turner-Foster, M. Lipson, and A. L. Gaeta, "Silicon-chip-based ultrafast optical oscilloscope," Nature **456**, 81–84 (2007).
13. Y. Dai, X. Chen, Y. Okawachi, A. C. Turner-Foster, M. A. Foster, M. Lipson, A. L. Gaeta, and C. Xu, "1 μs tunable delay using parametric mixing and optical phase conjugation in Si waveguides," Opt. Express **17**, 7004–7010 (2009).
14. H. K. Tsang, C. S. Wong, T. K. Liang, I. E. Day, S. W. Roberts, A. Harpin, J. Drake, and M. Asghari, "Optical dispersion, two-photon absorption and self-phase modulation in silicon waveguides at 1.5 μm wavelength," Appl. Phys. Lett. **80**, 416–418 (2002).
15. M. Dinu, F. Quochi, and H. Garcia, "Third-order nonlinearities in silicon at telecom wavelengths," Appl. Phys. Lett. **82**, 2954–2956 (2003).
16. G. W. Rieger, K. S. Virk, and J. F. Young, "Nonlinear propagation of ultrafast 1.5 μm pulses in high-index-contrast silicon-on-insulator waveguides," Appl. Phys. Lett. **84**, 900–902 (2004).
17. O. Boyraz, T. Indukuri, and B. Jalali, "Self-phase-modulation induced spectral broadening in silicon waveguides," Opt. Express **12**, 829–834 (2004).
18. A. R. Cowan, G. W. Rieger, and J. F. Young, "Nonlinear transmission of 1.5 μm pulses through single-mode silicon-on-insulator waveguide structures," Opt. Express **12**, 1611–1621 (2004).
19. H. Yamada, M. Shirane, T. Chu, H. Yokoyama, S. Ishida, and Y. Arakawa, "Nonlinear-optic silicon-nanowire waveguides," Jpn. J. Appl. Phys. **44**, 6541–6545 (2005).
20. I. Hsieh, X. Chen, J. I. Dadap, N. C. Panoiu, R. M. Osgood, Jr., S. J. McNab, and Y. A. Vlasov, "Ultrafast-pulse self-phase modulation and third-order dispersion in Si photonic-wire waveguides," Opt. Express **14**, 12380–12387 (2006).
21. L. Yin and G. P. Agrawal, "Impact of two-photon absorption on self-phase-modulation in silicon waveguides," Opt. Lett. **32**, 2031–2033 (2007).
22. S. Afshar V., W. Q. Zhang, H. Ebendorff-Heidepriem, and T. M. Monro, "Small core optical waveguides are more nonlinear than expected: experimental confirmation," Opt. Lett. **34**, 3577–3579 (2009).
23. S. Afshar V. and T. M. Monro, "A full vectorial model for pulse propagation in emerging waveguides with subwavelength structures part 1: Kerr nonlinearity," Opt. Express **17**, 2298–2318 (2009).
24. J. B. Driscoll, X. Liu, S. Yasseri, I. Hsieh, J. I. Dadap, and R. M. Osgood, Jr., "Large longitudinal electric fields (E_z) in silicon nanowire waveguides," Opt. Express **17**, 2797–2804 (2009).
25. J. I. Dadap, N. C. Panoiu, X. Chen, I. Hsieh, X. Liu, C. Chou, E. Dulkeith, S. J. McNab, F. Xia, W. M. J. Green, L. Sekaric, Y. A. Vlasov, and R. M. Osgood, Jr., "Nonlinear-optical phase modification in dispersion-engineered Si photonic wires," Opt. Express **16**, 1280–1299 (2008).
26. A. W. Snyder and J. D. Love, *Optical Waveguide Theory* (Kluwer Academic, 2000).
27. P. N. Butcher and D. Cotter, *The Elements of Nonlinear Optics* (Cambridge U. Press, 1990).
28. J. Zhang, Q. Lin, G. Piredda, R. W. Boyd, G. P. Agrawal, and P. M. Fauchet, "Anisotropic nonlinear response of silicon in the near-infrared region," Appl. Phys. Lett. **91**, 071113 (2007).
29. Q. Lin, J. Zhang, G. Piredda, R. W. Boyd, P. M. Fauchet, and G. P. Agrawal, "Dispersion of silicon nonlinearities in the near infrared region," Appl. Phys. Lett. **91**, 021111 (2007).
30. R. A. Soref and B. R. Bennett, "Electrooptical effects in silicon," IEEE J. Quantum Electron. **QE-23**, 123–129 (1987).
31. X. Chen, N. C. Panoiu, and R. M. Osgood, Jr., "Theory of Raman-mediated pulsed amplification in silicon-wire waveguides," IEEE J. Quantum Electron. **42**, 160–170 (2006).
32. G. P. Agrawal, *Nonlinear Fiber Optics* (Academic, 2007).
33. P. Lüsse, P. Stuwe, J. Schüle, and H. G. Unger, "Analysis of vectorial mode fields in optical waveguides by a new finite difference method," J. Lightwave Technol. **12**, 487–494 (1994).
34. M. Born and E. Wolf, *Principles of Optics* (Cambridge U. Press, 2005).